



Real-time, dynamic monitoring of selectively driven ion-concentration polarization

Matthew T. Flavin^{a,b}, Charles A. Lissandrello^b, Jongyoon Han^{*,a,c}

^a Department of Electrical Engineering and Computer Science, Massachusetts Institute of Technology, Cambridge, MA, United States

^b The Charles Stark Draper Laboratory, Inc., Cambridge, MA, United States

^c Department of Biological Engineering, Massachusetts Institute of Technology, Cambridge, MA, United States

ARTICLE INFO

Keywords:

Ionophore
Ion-selective membrane
Scanning electrochemical microscopy
Over-limiting

ABSTRACT

Selective ion extraction is a vital element of many resource recovery systems. Carrier-based membranes offer the ability to remove specific, targeted ions from brine and waste streams, but these materials have delivered inconsistent outcomes in their active transport applications. To study non-ideal behaviors of target-ion selective membranes, we introduce a direct, real-time system for selectively measuring concentrations within electro-membrane boundary layers. In a carrier-based membrane system, we applied our method to monitor adverse, current-limiting behaviors. During its operation, we detected loss of transport selectivity and counter-ion discharge. It provided sufficient evidence to identify the mechanism underlying these adverse, over-limiting effects—the internal concentration polarization of free-carrier. Our method may raise new prospects for direct experimental characterization of nonlinear transport phenomena in electro-membrane systems.

1. Introduction

Selective ion extraction, a vital element of many resource recovery systems, relies on membrane-based technologies. Eminent among these, is the ion-exchange membrane, which can selectively transport aqueous ions under the driving force of electric current. Its charge-based selectivity (permselectivity) makes this membrane essential in many important applications, including desalination [1] and biosensing [2]. Ion-exchange and ion-selective membranes are also an important component of photocatalysis applications, including fuel cells [3], organic dye degradation [4], and CO₂ reduction [5]. Recently, new applications have emerged that require not just charge-selectivity, but target-ion selectivity [6–10].

In our work, target-ion selectivity refers to the ability of a membrane to transport one particular ion within an electrolyte while blocking all others (i.e. single-ion selectivity). This ability has long been sought as a means of removing specific, targeted ions from brine and waste streams [1]. Recently, it has found new applications in bioelectronic chemical delivery [11]. In this study, which focuses on unique phenomena associated with target-ion selective membranes, we introduce an in situ monitoring system that revealed adverse, performance-limiting behaviors.

Ion-exchange membranes can selectively extract a single ion when it is being separated from other ions with different valences—such as Na⁺ in the presence of Ca²⁺ [1,12]. Meanwhile, when the selected ion is among those of identical charge, the only generalized method for creating a membrane with target-ion selectivity is by incorporating reactive carriers that reversibly bind with the selected ion. The liquid membrane offers the most flexible platform for compartmentalizing lipophilic carriers (ionophores). A wide range of carriers, originally developed for concentration sensing applications [13], are compatible with active, electrically driven operation [14–16]. However, for the purposes of active transport, these carrier-based membranes face unique and unresolved challenges.

In contrast with ion-exchange membranes, few instances of active transport with carrier-based membranes have materialized in the literature [11,17,18]. Qian et al. demonstrated the selective removal of Na⁺ from the drainage water of greenhouses [17], and Song et al. the localized modulation of Ca²⁺, Na⁺, and K⁺ in neural tissue [11]. Qian et al. ultimately found that the use of a Na⁺-selective carrier actually reduced their membrane's transport selectivity for Na⁺ over K⁺. While Song et al. observed no such performance loss in their study, we found that another adverse phenomenon may arise in this membrane, undetected by current methodologies. Its implications have broad relevance

* Corresponding author at: Department of Biological Engineering, Massachusetts Institute of Technology, Cambridge, MA, United States.

E-mail address: jyhan@mit.edu (J. Han).

<https://doi.org/10.1016/j.electacta.2022.140770>

Received 4 May 2022; Received in revised form 6 June 2022; Accepted 24 June 2022

Available online 1 July 2022

0013-4686/© 2022 Elsevier Ltd. All rights reserved.

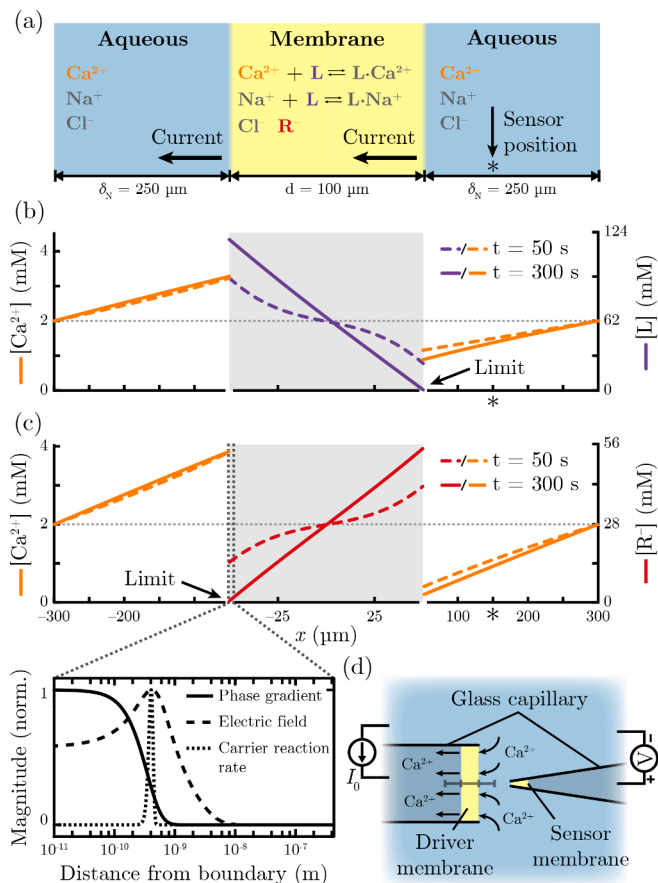


Fig. 1. Physicochemical model of solute transport within a carrier-based liquid membrane (SM lists default parameters). (a) Schematic illustration of model geometry (L is the carrier and R⁻ the lipophilic counter-ion). (b–c) Simulated concentration profiles of aqueous and membrane-confined solutes during constant current (transient and near-steady-state shown by dashed and solid lines respectively), given conditions that give rise to (b) the exhaustive depletion of free (unbound) carrier within the membrane (default parameters, -1 A/m^2 current density) and (c) the exhaustive depletion of lipophilic counter-ion ($D_L^{\text{org}} = 2 \times 10^{-11} \text{ m}^2/\text{s}$, -1.5 A/m^2 current density). The inset shows relative magnitudes of key interfacial processes that underlie characteristic membrane transport, normalized to their maximums within the depicted region. (d) Schematic illustration of direct concentration measurements (gray bar corresponds to the model geometry). The sensors and drivers had tip diameters $75\text{--}100 \mu\text{m}$ and $860 \mu\text{m}$ (inner) respectively.

to membrane systems, and the underlying process may account for the paradoxical outcome reported by Qian et al. (revisited in our conclusions).

From the work of investigators such as Rubinstein, Zaltzman, and Bazant, we now understand that intensive current conduction in ion-exchange membranes leads to over-limiting processes such as electroconvection [19,20] and water-splitting [21]. These processes pose challenges for most applications [21] but enable others, such as nano-fluidic preconcentration [22]. Meanwhile, the effect of these limiting mechanisms on target-ion selectivity is not well defined. This is particularly true for the carrier-based membrane, which is unique in that its constituents (the lipophilic carrier and counter-ion) are mobile, albeit confined by hydrophobicity. As we demonstrate in this article, intra-membrane processes can dominate as the limiting mechanism in this system and may underlie the inconsistent performances reported in previous studies.

The limiting behaviors of ion-exchange and carrier-based membranes arise from dynamic changes in boundary layer processes. In order to resolve their valuable temporal detail, we developed a method for

real-time, in situ monitoring of ion concentrations directly adjacent to a membrane during its operation.

Along with aqueous ions, our system directly detects lipophilic ions that can escape from membranes as harmful, performance-limiting electrochemical byproducts. For the first time, this method revealed that one intra-membrane processes causes the lipophilic counter-ion to rapidly discharge from carrier-based membranes under electrical polarization. Mechanistically, this current-driven behavior arises from relaxation of the membrane's boundary potential. This is distinct from the slow leaking of membrane components that develops over time under zero-current conditions [23]. Counter-ion discharge has remained undetected through currently available methods developed for concentration sensing, which include potentiometric, amperometric, and coulometric techniques [24–26]. This discharge poses a risk to any application of this type of membrane for active transport.

Selective measurements of ion concentrations with scanning electrochemical methodologies are limited in that they require zero-current conditions at the active surface [27–31]. Under electrical polarization, only non-selective measurements are possible [32,33]. To enable these measurements for electro-membrane systems, we drew inspiration from an electrophysiological technique, the discontinuous voltage clamp. To remove ohmic contamination, we operated the sensor and driver on a time-sharing basis. Our results with this system represent the first direct, local, selective concentration measurements of electrically driven ion concentration polarization.

2. Theory

As part of our previous work, we developed a model that simulates electrical polarization of carrier-based membranes [34]. In the present work, we apply predictions from this model to guide our experimental investigation. For a 1–D geometry, schematically illustrated in Fig. 1(a), the time-varying behavior of solute transport is dictated by continuity:

$$\frac{\partial c_i}{\partial t} + \frac{\partial N_{i,x}}{\partial x} = 0, \quad (1)$$

with c_i as the molar concentration and $N_{i,x}$ the xcomponent of the molar flux density of solute i . Chemical flux of each solute from diffusion and migration is given by the Nernst–Planck equations for dilute solutions:

$$N_{i,x} = -D_i \left(\frac{\partial c_i}{\partial x} + \frac{z_i F}{RT} c_i \frac{\partial V}{\partial x} \right), \quad (2)$$

where V is the electric potential, D_i is the diffusion coefficient of solute i , and z_i is the charge number of solute i . Meanwhile F , R , and T hold their usual meanings as Faradays constant, the universal gas constant, and absolute temperature respectively. The electric potential couples to the space charge density through Poissons equation:

$$\frac{\partial E_x}{\partial x} = -\frac{\partial^2 V}{\partial x^2} = \frac{F}{\epsilon_0 \epsilon_r} \sum_i z_i c_i, \quad (3)$$

where E_x is the xcomponent of the electric field, ϵ_0 is the permittivity of free space, and ϵ_r is the relative permittivity. The electric current density is defined as

$$J_x = F \sum_i z_i N_{i,x}. \quad (4)$$

In the membrane phase, the following reversible reactions describe carrier binding:



where L is the carrier, Ca^{2+} is the primary ion, Na^+ is an interfering ion, and n_i is the number of carrier molecules that bind to a single ion in a

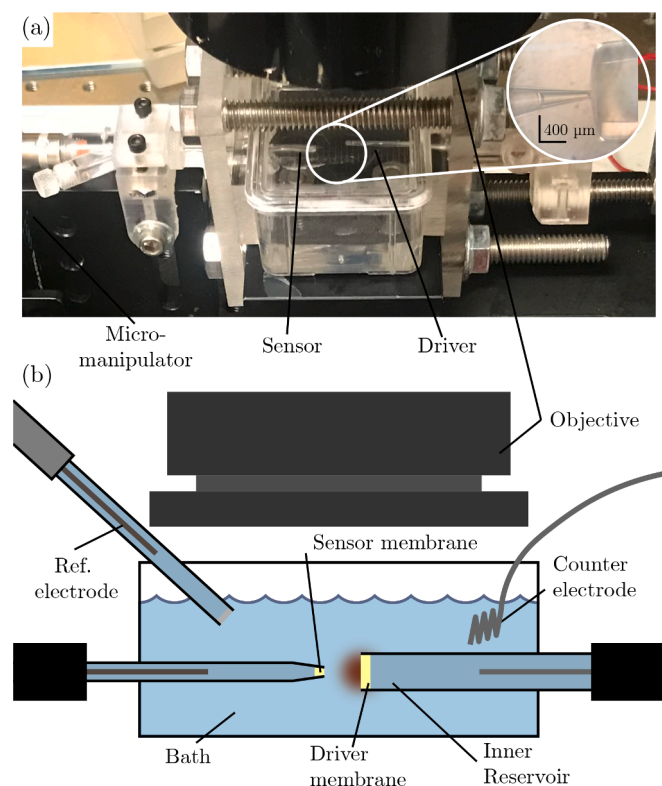


Fig. 2. Experimental setup for direct concentration measurements. (a) Photograph of experimental setup. The inset shows the tips of the sensor and driver electrodes aligned under a microscope. (b) Schematic illustration of experimental setup. The zero-current potential across the sensor membrane was measured between an Ag|AgCl electrode inserted into its inner reservoir and an Ag|AgCl|3.0M KCl reference electrode. Current was applied across the driver membrane between a platinum wire inserted into its inner reservoir and the counter-electrode, another platinum wire.

particular complex. In this model, these reactions were implemented as interior boundary conditions. For boundary conditions and parameters, see SM. Further discussion on this model can also be found in our previous article [34].

3. Experimental

3.1. Direct concentration measurements

To understand the interplay between the intra-membrane processes described by our model, we applied our monitoring system to detect temporal changes in their adverse effects. Our method employs two primary elements: (1) an electrochemically active surface, and (2) a sensor electrode acting as a probe to measure concentrations local to that surface. In this respect, our approach is related to scanning electrochemical microscopy.

In our case, the electrochemically active surface (1) is a carrier-based membrane embedded in the tip of a glass capillary (860 μm inner diameter), and we refer to this as the driver membrane. Meanwhile, the sensor electrode (2) is another ion-selective membrane embedded in the tip of a glass micropipette (75–100 μm tip diameter). Fig. 2 shows the sensor and driver, positioned tip-to-tip by micromanipulators. In this configuration, we could apply zero-current potentiometry at the sensor electrode to measure concentrations within micrometers of the surface of the driver membrane. Prior literature report that sensor response times for each of the ionophores used in this study were within 85 ms [35,36].

Our electrochemical cell comprised of an electrolyte bath of 2 mM

CaCl_2 , 100 mM NaCl, 10 mM KCl, and 25 mM HEPES, adjusted to 7.4 pH using NaOH. In addition to the driver and sensor membranes, the cell contained an Ag|AgCl|3.0 M KCl reference electrode and a platinum wire counter-electrode. Current was applied across the driver membrane between a platinum wire inserted into its inner reservoir and the counter-electrode. The zero-current EMF across the sensor membrane was measured between an Ag|AgCl electrode inserted into its inner reservoir and the reference electrode. The inner reservoirs of both the sensor and driver were comprised of the same media as the electrolyte bath. The potential across the sensor membrane was measured with a Keithley 6514 Electrometer, using a guarded line to prevent parasitic capacitances. In order to shield the cell from external noise, the sensor ground was connected to a uniform conducting plate that laid directly underneath the system. The current was applied across the driver membrane from one of the channels of a Keithley 2612B SourceMeter.

The driver and sensor were inserted horizontally at diametric ends of the electrochemical cell through flexible silicone gaskets. Their tips were positioned to the correct distances under the objective of an Olympus SZX16 microscope. The tip-to-tip distances were determined from an eyepiece reticle.

3.2. Ion selective electrode materials and fabrication

Both the driver and sensor electrodes were fabricated from borosilicate glass capillaries (1.5 mm outer diameter, 860 μm inner diameter; Sutter Instrument). Filamented glass was used only for the Ca^{2+} sensors. The glass capillaries of the sensors were pulled and then broken to tip diameters of 75–100 μm , and those of the drivers were left at their original diameters. Before inserting the membrane cocktails, each capillary was silanized using 5% dimethyldichlorosilane in heptane (Selectophore, Supelco).

The driver membrane was Ca^{2+} -selective in all cases, and the sensors were either Ca^{2+} -, Na^+ -, or K^+ -selective. As shown in Table SM-2, each formulation was based on those reported in prior literature. The constitutive elements of each were purchased from Selectophore, Supelco.

We would immerse the capillary for each driver into the appropriate cocktail such that a 2mm column of the cocktail solution entered the shaft. The tetrahydrofuran (THF) of the cocktail was allowed to evaporate over 10min, and then we backfilled the capillary with the inner reservoir solution. After evaporation and dissolution of the THF, the final thickness of the column was 100 μm . The capillary would then be fully immersed in electrolyte (of identical composition to the inner reservoir) and allowed to equilibrate for 24–32 h prior to experiment.

For the sensors, each capillary would first be backfilled with the inner reservoir solution. Then, the tips would be immersed in the cocktail solution such that columns of 1 mm entered the shanks. For the PVC-based membranes, each capillary would be immersed in electrolyte (of identical composition to the inner reservoir) and allowed to equilibrate for 24–32 h prior to experiment. After dissolution of THF, the column of the membrane would shrink to 100–150 μm . For each of the non-PVC membranes, the electrode would be prepared immediately prior to an experiment without prolonged equilibration.

4. Results and discussion

4.1. Physicochemical modeling

We applied predictions from a physicochemical transport model to guide our investigation of a carrier-based membrane system. The governing equations of Nernst–Planck–Poisson render concentration profiles that form in both the aqueous and membrane domains. Just as for ion-exchange membranes, these diffusion boundary layers (concentration polarization) develop as a result of driving ions across boundaries between domains with mismatched transport characteristics [37]. Because of the mismatch in the selected ion's mobility between the

Table 1
Membrane current-limiting processes (derived in SM).

Limiting process	I_0 (μA) ^a	τ_{eq} (s) ^b	Adverse effect
Membrane depletion of free carrier, Fig. 1(b)	–	10^3	Loss of target-ion selectivity Egress of lipophilic counter-ion
Membrane depletion of lipophilic counter-ion, Fig. 1(c)	+	10^3	Loss of charge selectivity
Aqueous depletion of ions	–	10^1	Loss of target-ion selectivity
Carrier reaction kinetics	–	10^{-11}	Loss of target-ion selectivity

^a Direction of current that gives rise to the limiting process (with respect to instrumentation shown in Fig. 1[d]).

^b Equilibrium time-constant, order of magnitude based on model.

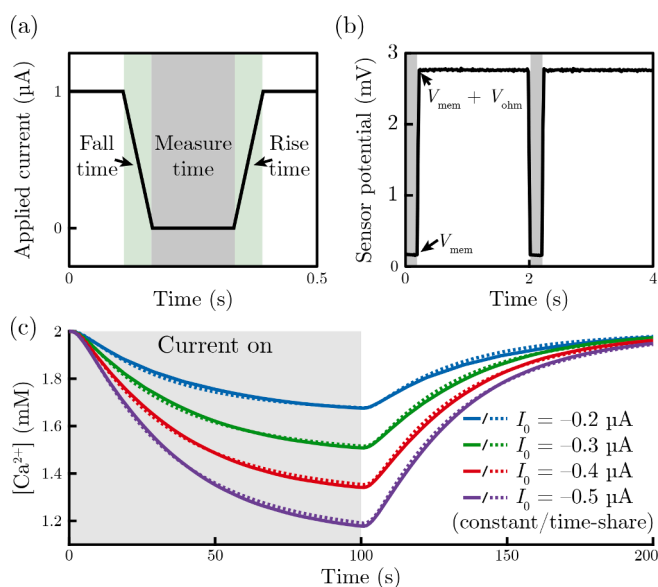


Fig. 3. Principles of time-sharing measurements. (a) Waveform of current applied to the driver membrane. (b) Raw potential measured from the sensor amidst the application of current at the driver. During the short intervals denoted as the Measure time, the current is shut off and a measurement is taken (timed to avoid the rise and fall times). During this interval, the sensor potential reflects the boundary potentials across the membrane rather than that combined with the ohmic potential drop generated by the external current (i.e. the sensor indicates V_{mem} during the \otimes Measure time and $V_{\text{mem}} + V_{\text{ohm}}$ when the current is resumed). (c) Simulation of Ca^{2+} measurements comparing constant galvanostatic polarization (solid lines) and time-sharing (dashed lines), with current applied during the first 100 s.

phases, as shown in Fig. 1(b) and (c), electric current (I_0) causes boundary layers of that ion (Ca^{2+}) to form in the aqueous regions sandwiching the membrane (Fig. 1[d] illustrates the direction of current).

There is, likewise, a mismatch in the transport of membrane species—the carrier (L) and lipophilic counter-ion (R^-)—as neither are present in substantive concentrations in the aqueous phase outside the membrane. Thus, as shown in Fig. 1(b) and (c), in a manner similar to Ca^{2+} in the aqueous regions, intra-membrane L and R^- undergo concentration polarization. These intra-membrane phenomena have previously been observed in experiments using spectroelectrochemical microscopy [38,39]. With our in situ measurement system, we aimed to monitor how this intra-membrane concentration polarization affects over-limiting transport behaviors, discharge and selectivity loss included.

In Table 1, we summarize the current-limiting processes our model predicts will impair the operation of a carrier-based membrane in a

practical system (see SM for derivation). Caused by aqueous and intra-membrane concentration polarization, each process can dominate depending on the exact properties of the membrane. Critical properties, such as intra-membrane diffusion coefficients, are part of an immense and sparsely determined parameter space. The effect of each process intensifies as concentrations approach exhaustion at either boundary of the membrane. The time-scale differs for each effect, as does the polarity of current that gives rise to it. According to our model, each process will reduce the transport selectivity of the membrane with respect to either interfering co-ions or counter-ions, given a sufficiently large current. For one of the given processes—that caused by concentration polarization of free, unbound carrier—the model indicates that the rapid discharge of lipophilic counter-ion will occur. This discharge, driven by relaxation of the interface's energetic barrier, not only causes loss of function but also introduces harmful byproducts into the media.

4.2. Direct concentration measurements

Scanning electrochemical methodologies [27–33] are limited in that they require zero-current conditions at the active surface for ion-selective measurements. Electrical current applied through the active surface produces ohmic contamination in the sensor reading. To enable these measurements for electro-membrane systems, we drew inspiration from an electrophysiological technique, the discontinuous voltage clamp. To remove ohmic contamination, we operated the sensor and driver on a time-sharing basis. Repetitively, under instrument control, the driver would be switched off to allow the sensor membrane to take a measurement and then switched back on immediately after.

As shown in Fig. 3(a) and (b), the measurement would be initiated in the narrow window between the rise and fall times of the current source. The rise and fall times arise from transient features, such as instrument capacitance. Based on continuous measurements, shown in Fig. 3(b), we determined that the potential reached quasi-steady-state (with respect to the slower time-scale of diffusion boundary layer formation) within 67 ms of transitioning from constant current to zero current. For a 2 s period in between measurements and a 167 ms measure time, the simulation shown in Fig. 3(c) indicates that only negligible differences exist between the effects of constant current and the effects of time-sharing (for calibration and parameters, see SM). Therefore, we chose a 167 ms measure time in our experiments to isolate the temporal dynamics of diffusion boundary layer formation in our measurements.

To study a carrier-based membrane, we positioned the sensor microelectrode within a fixed distance, 100 μm , from the tip of the driver membrane (illustrated in Figs. 1[d] and 2[b]). The sensor electrode—either Na^+ , K^+ , or Ca^{2+} -selective in our study—would perform zero-current potentiometric concentration measurements within the aqueous diffusion boundary layer of the driver. Transfer selectivity, quantified by integral transference, varies directly with the selected ion's concentration within this boundary layer (given excess supporting electrolyte). Thus, as demonstrated below, these local measurements allowed us to detect changes in transfer selectivity.

Simultaneously, our method detected counter-ion discharge, which, along with selectivity loss, is an adverse effect predicted by our model. The sensor membrane, identical to the driver, absorbs lipophilic elements with high affinity. Therefore, without requiring any explicit carriers for the lipophilic counter-ion, its presence manifested in the sensor potential as a sudden, massive shift towards negative polarity (for an anion). We found that this feature was easily discernible in real-time, occurring on a time-scale and to an extent that eliminated all other known ions in the system as its potential cause. As verified below, this principle allowed us to perform binary detection of counter-ion discharge.

4.3. Monitoring adverse transport behavior

The simultaneous detection of counter-ion discharge and loss of

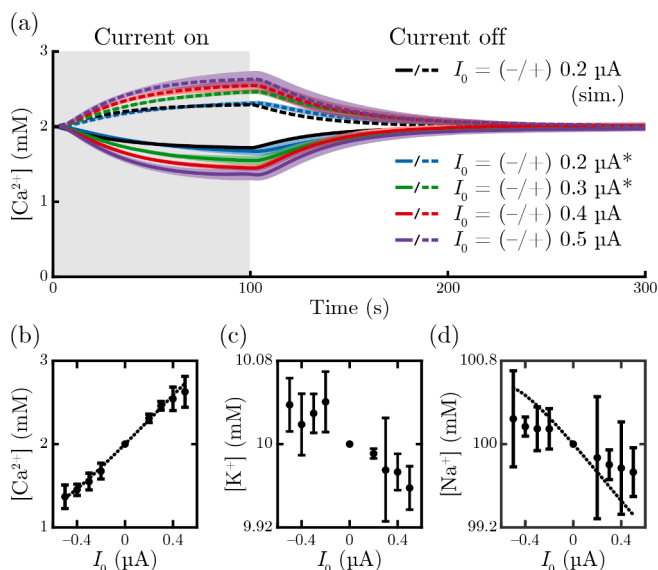


Fig. 4. Direct concentration measurements of aqueous ions measured 100 μm from the surface of the driver membrane (bath containing 10 mM KCl). (a) Temporal profile of Ca^{2+} concentration during and after applied current (shaded regions show standard deviations, $n = 4$ and $*n = 3$ independent sensor/driver pairs; black lines show simulation results from default parameters; solid and dashed lines correspond to negative and positive currents respectively). (b–d) Concentrations of Ca^{2+} (b), K^+ (c), and Na^+ (d) measured at 100 s ($n = 3$ sensor/driver pairs for K^+ and Na^+ ; dotted lines show simulation results from default parameters).

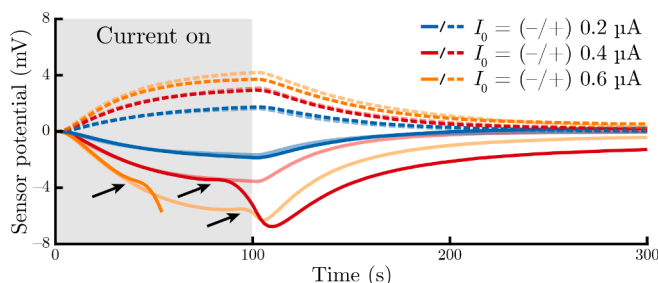


Fig. 5. Raw potential readings from the Ca^{2+} -selective sensor demonstrating conditions that give rise to tetrabutylborate discharge. The raw potential is logarithmically related to the sensed concentrations. The solid-colored and faded lines show measurements taken with 10 mM KCl and 0 mM KCl respectively. The arrows indicate features associated with the detection of tetrabutylborate. Upon detection of the lipophilic counter-ion, the potential returns more slowly back to equilibrium.

transport selectivity provided us with a direct means of evaluating a carrier-based membrane system in terms of the current-limiting processes listed in Table 1.

We focused our study on the membrane system reported by Song et al. (as the driver membrane), a plasticized polymer formulated with a Ca^{2+} -selective carrier and tetrabutylborate (TPB^-) as the lipophilic counter-ion [11]. The bath electrolyte contained Ca^{2+} , Na^+ , K^+ , and Cl^- .

The system's behavior conformed to modeling predictions. It was consistent between independent sensor/driver pairs as well as successive operations on each pair. As Fig. 4(a) and (b) demonstrate, the concentration varied directly with applied current, both positive and negative. At the same time, Fig. 4(c) and (d) show that the changes in K^+ and Na^+ were nearly negligible and varied inversely with the level of current. These relationships, predicted in our simulations, are characteristic of ideal, near-equilibrium selectivity. Thus, we could apply a current of $-0.5 \mu A$ for at least 100 s without encountering noticeable

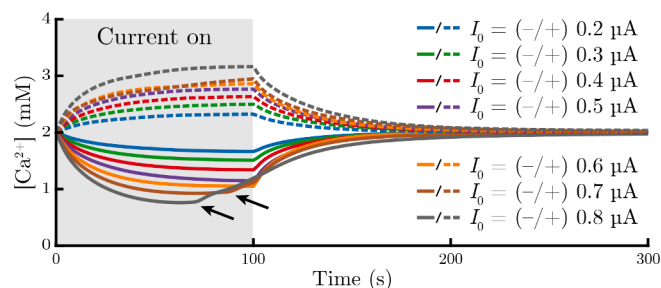


Fig. 6. Direct concentration measurements of Ca^{2+} concentration measured 100 μm from the surface of a driver membrane containing tetrakis(4-chloro)phenylborate as the lipophilic counter-ion (bath containing 10 mM KCl); representative of $n = 4$ sensor/driver pairs). The arrows indicate features associated with loss of transport selectivity.

deviations from ideal transport.

Beyond the regime of Fig. 4, however, we began to see clear evidence of current-limiting behavior. As shown in Fig. 5, after applying a current of $-0.6 \mu A$, the boundary potential transitioned sharply and negatively at 96 s (87.5 ± 7.7 s, $n = 4$ electrode pairs), after the measurement was already approaching a steady-state. We found that if the current was not terminated early in this process, the boundary potential of each sensor, regardless of its selected ion, would rapidly shift by more than 100 mV. Based on conservative estimates of aqueous concentration polarization, this far exceeds what the hydrophilic ions, Ca^{2+} , K^+ , H^+ , Na^+ , and Cl^- , would be capable of under any current regime we tested. Meanwhile, under positive polarity of current at the same magnitude, we observed no deviation from ideal transport. These characteristics indicate the detection of TPB^- , considering the previously outlined criteria.

In order to verify our method, its detection of lipophilic counter-ion, we repeated the Ca^{2+} measurements in the absence of K^+ . As TPB^- forms ion pairs with K^+ in aqueous media, its influence should vary according to the presence of K^+ [40]. As shown in Fig. 5, with 0 mM KCl in the bath electrolyte, we detected TPB^- after applying currents of only $-0.4 \mu A$ for 86 s (81 ± 8.4 s, $n = 4$ electrode pairs). The presence of K^+ clearly had an effect on the ions detected by our sensors, despite the fact that the concentration of K^+ itself remained nearly constant during the experiments in which it was present (shown in Fig. 6[c]). Our results agree with the intuition that K^+-TPB^- association would reduce the availability of free TPB^- and effectively limit its transport in the aqueous phase. Thus, the effect of changing bath KCl concentrations confirms that the driver electrode discharged TPB^- during its polarization.

As the discharge of TPB^- poses a significant threat to selective ion transport, we then applied our direct measurement technique to identify an approach for mitigating it. For another set of experiments, we replaced TPB^- with tetrakis(4-chlorophenyl)borate ($TKClPB^-$) as the driver membrane's lipophilic counter-ion. The lipophilicity, quantified by the partition coefficient, of $TKClPB^-$ is an order of magnitude greater than that of TPB^- . This property has been shown to improve the lifetime of zero-current membrane sensors [23]. While the TPB^- membrane could only sustain up to $-0.5 \mu A$ without discharging within 100 s, Fig. 6 shows that we detected no discharge of $TKClPB^-$ under any of the conditions we tested, with currents up to $-0.8 \mu A$. Neither did we observe any discharge after removing KCl from the bath.

Although we detected no counter-ion discharge from the improved membrane, the Ca^{2+} sensor did detect a loss in transport selectivity that became noticeable suddenly upon approaching $-0.8 \mu A$ (indicated by arrows in Fig. 6). This phenomenon arose after applying $-0.7 \mu A$ for 78.5 ± 9.6 s or $-0.8 \mu A$ for 65.5 ± 6.6 s (across four independent electrode pairs).

4.4. Identifying current-limiting processes

The available evidence indicates that free-carrier concentration po-

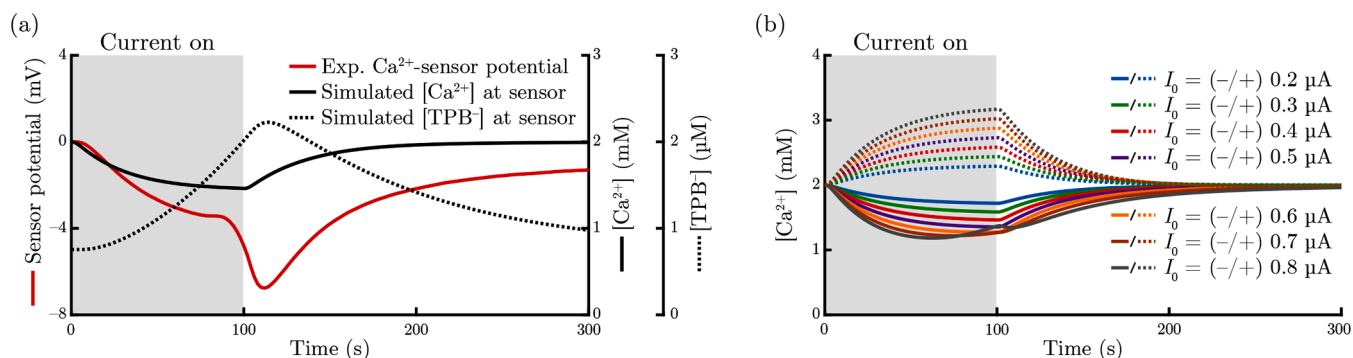


Fig. 7. Simulations of current-limiting behaviors, their effects on the sensor electrode. (a) Simulated concentrations of Ca²⁺ and TPB⁻ measured 100 μm from the surface of the driver membrane (applying -0.4 μA). Plotted on the same axis, is the raw sensor readings from our experiment with the Ca²⁺-selective sensor (applying -0.4 μA). This behavior arises from relaxation of the membrane's boundary potential. (b) Simulation of Ca²⁺ concentration measured 100 μm from the surface of the driver membrane ($\log K_R^{\text{part}} = -5$). The partition coefficient was scaled by an order of magnitude to mimic the effect of replacing TPB⁻ with TKClPB⁻.

larization dominated as the limiting mechanism for both membranes examined here (see Fig. 1[b] and Table 1, first row). The influence of the aqueous boundary layer is not feasible, as we maintained all currents across the TPB⁻ membrane well within the aqueous limit for Ca²⁺, $J_{\text{lim}}^{\text{Ca}^{2+}} = -1.22 \text{ A/m}^2$ (calculation in SM). In addition, we can disregard the reaction boundary layer [34], whose effect would arise nearly instantaneously rather than over 100 s. Between the lipophilic counter-ion and free carrier, only concentration polarization of the latter agrees with our observations that the non-ideal behavior occurs under negative polarity and not positive. Finally, the free-carrier boundary layer is the only process that our model predicts can lead to the discharge of TPB⁻. Crucially, this limiting mechanism also accounts for the loss of transport selectivity in the TKClPB⁻ membrane. We conclude that free-carrier concentration polarization dominated as the limiting mechanism, that it caused discharge and selectivity loss. This current-driven behavior arises from the relaxation of the membrane's boundary potential and does not involve chemical deterioration.

These results support the findings of Ref. [24], which attributed polarization of both free carrier and lipophilic counter-ion to distinct chronopotentiometric breakpoints. On the same time-scale as these breakpoints, we observed loss of transport selectivity and counter-ion discharge. Both our model and that of Ref. [24] predict that this loss of transport selectivity at the boundary where current enters the membrane would arise from polarization of free-carrier.

Both the loss of transport selectivity and discharge were clearly recapitulated by our model. With intra-membrane diffusion coefficients of the carrier and lipophilic counter-ion taken within the range of published values [41], we found excellent agreement in the relative timings of all adverse phenomena between the experimental (Figs. 5 and 6) and theoretical (Fig. 7) results. Extrapolating from our results, the TKClPB⁻ membrane should sustain, at steady-state, currents up to 0.46 μA without losing selectivity. If currents in excess of this limit are applied for a sufficiently long duration, the model predicts that, despite its improved lipophilicity, TKClPB⁻ will discharge from the membrane.

5. Conclusions

In conclusion, our source-measurement time-sharing technique presents an effective means of identifying adverse phenomena affecting the target-ion selectivity of a carrier-based membrane. In our study, it yielded the first evidence of rapid, driven discharge of lipophilic counter-ion. This evidence supports the predictions of our model, which indicate that this discharge arises from relaxation of the membrane's boundary potential. The detection of discharge and loss of transport selectivity provided sufficient evidence to positively identify their underlying cause—the intra-membrane concentration polarization of free-carrier—and its temporal onset.

Our model, which we previously examined in Ref. [34], was able to recapitulate the current-limiting processes we examined here, along with their adverse effects. While this model suggests that a reaction boundary layer may arise under some conditions and prevent effective operation, we did not observe evidence for this phenomenon under the conditions we examined here.

The effects of free-carrier concentration polarization provide a possible explanation for the paradoxical results of Qian et al., who also found that their carrier-based liquid membrane failed to selectively transport its primary ion under intensive currents [17]. In addition, guided by our method, we improved on the membrane of Song et al. [11] by modifying its composition, eliminated its discharge under the regime that we studied.

Discharge of lipophilic counter-ion and loss of transport selectivity are fundamental to the operation of the membrane. Both will result in loss of function, and counter-ion discharge introduces harmful byproducts into the aqueous solution. This is likewise a factor for ion-exchange membranes. Through mechanisms chemical rather than energetic, their fixed charges can degrade into hydrophobic ions [42,43] under conditions that arise from intensive current [44].

Our method for direct, real-time, quantitative measurement of ion concentration raises new prospects for the study of electro-membrane systems. This type of measurement has not previously been possible within electrically driven boundary layers. It may elicit new perspectives on nonlinear transport phenomena such as current-induced membrane discharge [45] and equilibrium electroconvective instability [20], for which selectivity is a fundamental aspect. In application, it enables continuous, in situ monitoring of membrane performance and even closed-loop operation.

CRediT authorship contribution statement

Matthew T. Flavin: Conceptualization, Methodology, Validation, Writing – original draft. **Charles A. Lissandrello:** Conceptualization, Supervision, Project administration, Funding acquisition. **Jongyoon Han:** Conceptualization, Supervision, Project administration, Funding acquisition.

Declaration of Competing Interest

The authors declare that they have no known competing financial interests or personal relationships that could have appeared to influence the work reported in this paper.

Data Availability

Data will be made available on request.

Acknowledgments

The work presented in this article was supported, in part, by the Quick Faculty Innovation Fellowship of MIT. MF was supported by the Draper Scholars Program.

Supplementary material

Supplementary material associated with this article can be found, in the online version, at [10.1016/j.electacta.2022.140770](https://doi.org/10.1016/j.electacta.2022.140770)

References

- [1] T. Luo, S. Abdu, M. Wessling, Selectivity of ion exchange membranes: a review, *J. Memb. Sci.* 555 (2018) 429–454, <https://doi.org/10.1016/j.memsci.2018.03.051>.
- [2] R.J. Toh, W.K. Peng, J. Han, M. Pumera, Direct in vivo electrochemical detection of haemoglobin in red blood cells, *Sci. Rep.* 4 (2014) 6209, <https://doi.org/10.1038/srep06209>.
- [3] P.T. Nonjola, M.K. Mathe, R.M. Modibedi, Chemical modification of polysulfone: composite anionic exchange membrane with TiO₂ nano-particles, *Int. J. Hydrogen Energy* 38 (12) (2013) 5115–5121, <https://doi.org/10.1016/j.ijhydene.2013.02.028>.
- [4] Y.K. Manea, A.M. Khan, Enhanced photocatalytic degradation of methylene blue and adsorption of metal ions by SDS-TiP nanocomposite, *SN Appl. Sci.* 1 (8) 821.
- [5] G. Zeng, J. Qiu, B. Hou, H. Shi, Y. Lin, M. Hettick, A. Javey, S.B. Cronin, Enhanced photocatalytic reduction of CO₂ to CO through TiO₂ passivation of InP in ionic liquids, *Chemistry* 21 (39) (2015) 13502–13507, <https://doi.org/10.1002/chem.201501671>.
- [6] Y. Tanaka, R. Ehara, S. Itoi, T. Goto, Ion-exchange membrane electro-dialytic salt production using brine discharged from a reverse osmosis seawater desalination plant, *J. Memb. Sci.* 222 (1–2) (2003) 71–86, [https://doi.org/10.1016/S0376-7388\(03\)00217-5](https://doi.org/10.1016/S0376-7388(03)00217-5).
- [7] WHO, Desalination and water purification research and development zero discharge seawater desalination: integrating the production of freshwater, salt, magnesium, and bromine, Desalination and Water Purification Research and Development Program Report No. 111.
- [8] Z.y. Ji, Q.b. Chen, J.s. Yuan, J. Liu, Y.y. Zhao, W.x. Feng, Preliminary study on recovering lithium from high Mg²⁺/Li⁺ ratio brines by electro-dialysis, *Sep. Purif. Technol.* 172 (2017) 168–177, <https://doi.org/10.1016/j.seppur.2016.08.006>.
- [9] X.Y. Nie, S.Y. Sun, Z. Sun, X. Song, J.G. Yu, Ion-fractionation of lithium ions from magnesium ions by electro-dialysis using monovalent selective ion-exchange membranes, *Desalination* 403 (2017) 128–135, <https://doi.org/10.1016/j.desal.2016.05.010>.
- [10] J. Lambert, M. Avila-Rodriguez, G. Durand, M. Rakib, Separation of sodium ions from trivalent chromium by electro-dialysis using monovalent cation selective membranes, *J. Memb. Sci.* 280 (1–2) (2006) 219–225, <https://doi.org/10.1016/j.memsci.2006.01.021>.
- [11] Y.A. Song, R. Melik, A.N. Rabie, A.M. Ibrahim, D. Moses, A. Tan, J. Han, S.J. Lin, Electrochemical activation and inhibition of neuromuscular systems through modulation of ion concentrations with ion-selective membranes, *Nat. Mater.* 10 (12) (2011) 980–986, <https://doi.org/10.1038/nmat3146>.
- [12] T. Sata, T. Sata, W. Yang, Studies on cation-exchange membranes having permselectivity between cations in electro-dialysis, *J. Memb. Sci.* 206 (1–2) (2002) 31–60, [https://doi.org/10.1016/S0376-7388\(01\)00491-4](https://doi.org/10.1016/S0376-7388(01)00491-4).
- [13] E. Bakker, P. Bühlmann, E. Pretsch, Carrier-based ion-selective electrodes and bulk optodes. 1. General characteristics, *Chem. Rev.* 97 (8) (1997) 3083–3132, <https://doi.org/10.1021/cr940394a>.
- [14] G.A. Crespo, E. Bakker, Dynamic electrochemistry with ionophore based ion-selective membranes, *RSC Adv* 3 (2013) 25461–25474, <https://doi.org/10.1039/c3ra43751e>.
- [15] E. Grygolowicz-Pawlak, E. Bakker, Thin layer coulometry with ionophore based ion-selective membranes, *Anal. Chem.* 82 (11) (2010) 4537–4542, <https://doi.org/10.1021/ac100524z>.
- [16] M.G. Afshar, G.A. Crespo, E. Bakker, Direct ion speciation analysis with ion-selective membranes operated in a sequential potentiometric/time resolved chronopotentiometric sensing mode, *Anal. Chem.* 84 (20) (2012) 8813–8821, <https://doi.org/10.1021/ac302092m>.
- [17] Z. Qian, H. Miedema, S. Sahin, L.C. de Smet, E.J. Sudhölter, Separation of alkali metal cations by a supported liquid membrane (SLM) operating under electro-dialysis (ED) conditions, *Desalination* 495 (2020) 114631, <https://doi.org/10.1016/j.desal.2020.114631>.
- [18] A. Šlampová, P. Kubá, P. Boček, Fine-tuning of electromembrane extraction selectivity using 18-crown-6 ethers as supported liquid membrane modifiers, *Electrophoresis* 35 (23) (2014) 3317–3320, <https://doi.org/10.1002/elps.201400372>.
- [19] M.Z. Bazant, T.M. Squires, Induced-charge electrokinetic phenomena: theory and microfluidic applications, *Phys. Rev. Lett.* 92 (6) (2004) 66101, <https://doi.org/10.1103/PhysRevLett.92.066101>.
- [20] I. Rubinstein, B. Zaltzman, Equilibrium electroconvective instability, *Phys. Rev. Lett.* 114 (2015) 114502, <https://doi.org/10.1103/PhysRevLett.114.114502>.
- [21] V.V. Nikonenko, N.D. Pismenskaya, E.I. Belova, P. Sístat, P. Huguet, G. Pourcelly, C. Larchet, Intensive current transfer in membrane systems: modelling, mechanisms and application in electro-dialysis, *Adv. Colloid Interface Sci.* 160 (1–2) (2010) 101–123, <https://doi.org/10.1016/j.cis.2010.08.001>.
- [22] S.H. Ko, Y.-A. Song, S.J. Kim, M. Kim, J. Han, K.H. Kang, Nanofluidic preconcentration device in a straight microchannel using ion concentration polarization, *Lab Chip* 12 (2012) 4472–4482, <https://doi.org/10.1039/C2LC21238B>.
- [23] E. Bakker, E. Pretsch, Lipophilicity of tetraphenylborate derivatives as anionic sites in neutral carrier-based solvent polymeric membranes and lifetime of corresponding ion-selective electrochemical and optical sensors, *Anal. Chim. Acta* 309 (1–3) (1995) 7–17, [https://doi.org/10.1016/0003-2670\(95\)00077-D](https://doi.org/10.1016/0003-2670(95)00077-D).
- [24] J.M. Zook, S. Bodor, R.E. Gyurcsányi, E. Lindner, Interpretation of chronopotentiometric transients of ion-selective membranes with two transition times, *J. Electroanal. Chem.* 638 (2) (2010) 254–261, <https://doi.org/10.1016/j.jelechem.2009.11.007>.
- [25] V. Bhakthavatsalam, E. Bakker, Operational limits of controlled current coulometry with ion-selective polymeric membranes, *Electroanalysis* 20 (3) (2008) 225–232, <https://doi.org/10.1002/elan.200703979>.
- [26] B.D. Pendley, R.E. Gyurcsányi, R.P. Buck, E. Lindner, A chronoamperometric method to estimate changes in the membrane composition of ion-selective membranes, *Anal. Chem.* 73 (19) (2001) 4599–4606, <https://doi.org/10.1021/ac10007e>.
- [27] R.E. Gyurcsányi, E. Pergel, R. Nagy, I. Kapui, B.T. Lan, K. Tóth, I. Bitter, E. Lindner, Direct evidence of ionic fluxes across ion-selective membranes: a scanning electrochemical microscopic and potentiometric study, *Anal. Chem.* 73 (9) (2001) 2104–2111, <https://doi.org/10.1021/ac000922k>.
- [28] C. Wei, A.J. Bard, G. Nagy, K. Toth, Scanning electrochemical microscopy. 28. Ion-selective neutral carrier-based microelectrode potentiometry, *Anal. Chem.* 67 (8) (1995) 1346–1356, <https://doi.org/10.1021/ac00104a008>.
- [29] P. Dauphin-Ducharme, R.M. Asmussen, D.W. Shoesmith, J. Mauzeroll, In-situ Mg²⁺ release monitored during magnesium alloy corrosion, *J. Electroanal. Chem.* 736 (2015) 61–68, <https://doi.org/10.1016/j.jelechem.2014.10.030>.
- [30] H. Yamada, D. Haraguchi, K. Yasunaga, Fabrication and characterization of a K⁺-selective nanoelectrode and simultaneous imaging of topography and local K⁺ flux using scanning electrochemical microscopy, *Anal. Chem.* 86 (17) (2014) 8547–8552, <https://doi.org/10.1021/ac502444y>.
- [31] B.P. Nadappuram, K. Mc Kelvey, R. Al Botros, A.W. Colburn, P.R. Unwin, Fabrication and characterization of dual function nanoscale pH-scanning ion conductance microscopy (SICM) probes for high resolution pH mapping, *Anal. Chem.* 85 (17) (2013) 8070–8074, <https://doi.org/10.1021/ac401883n>.
- [32] J.-H. Choi, J.-S. Park, S.H. Moon, Direct measurement of concentration distribution within the boundary layer of an ion-exchange membrane, *J. Colloid Interface Sci.* 251 (2) (2002) 311–317, <https://doi.org/10.1006/jcis.2002.8407>.
- [33] S. Mareev, D. Butylskii, N. Pismenskaya, C. Larchet, L. Dammak, V. Nikonenko, Geometric heterogeneity of homogeneous ion-exchange neosepta membranes, *J. Memb. Sci.* 563 (2018) 768–776, <https://doi.org/10.1016/j.memsci.2018.06.018>.
- [34] M.T. Flavin, D.K. Freeman, J. Han, Interfacial ion transfer and current limiting in neutral-carrier ion-selective membranes: a detailed numerical model, *J. Memb. Sci.* 572 (2019) 374–381, <https://doi.org/10.1016/j.memsci.2018.10.065>.
- [35] M. Huser, P.M. Gehrig, W.E. Morf, W. Simon, E. Lindner, J. Jeney, K. Tóth, E. Pungor, Membrane technology and dynamic response of ion-selective liquid-membrane electrodes, *Anal. Chem.* 63 (14) (1991) 1380–1386, <https://doi.org/10.1021/ac00014a009>.
- [36] J.C. Oceau, G. Faas, I. Mody, B.S. Khakh, Making, testing, and using potassium ion selective microelectrodes in tissue slices of adult brain, *J. Vis. Exp.* 135 (2018) 57511, doi:10.3791/57511.
- [37] M. Flavin, *Electrochemical Neuromodulation Using Electrodes Modified with Ion-Selective Materials, Based on the Physical Process of Ion-Concentration Polarization*, Massachusetts Institute of Technology, 2018. Master's thesis.
- [38] R.E. Gyurcsányi, E. Lindner, Spectroelectrochemical microscopy: spatially resolved spectroelectrochemistry of carrier-based ion-selective membranes, *Anal. Chem.* 77 (7) (2005) 2132–2139, <https://doi.org/10.1021/ac048445j>.
- [39] J.M. Zook, R.P. Buck, R.E. Gyurcsányi, E. Lindner, Mathematical model of current-polarized ionophore-based ion-selective membranes: large current chronopotentiometry, *Electroanalysis* 20 (3) (2008) 259–269, <https://doi.org/10.1002/elan.200704052>.
- [40] R.M. Engelbrecht, F.A. Mccoy, Determination of potassium by a tetraphenylborate method, *Anal. Chem.* 28 (11) (1956) 1772–1773, <https://doi.org/10.1021/ac60119a040>.
- [41] S. Bodor, J.M. Zook, E. Lindner, K. Tóth, R.E. Gyurcsányi, Electrochemical methods for the determination of the diffusion coefficient of ionophores and ionophore-ion complexes in plasticized PVC membranes, *Analyst* 133 (5) (2008) 635–642, <https://doi.org/10.1039/b718110h>.
- [42] G. Merle, M. Wessling, K. Nijmeijer, Anion exchange membranes for alkaline fuel cells: a review, *J. Memb. Sci.* 377 (1) (2011) 1–35, <https://doi.org/10.1016/j.memsci.2011.04.043>.
- [43] H. Tang, S. Peikang, S.P. Jiang, F. Wang, M. Pan, A degradation study of Nafion proton exchange membrane of PEM fuel cells, *J. Power Sources* 170 (1) (2007) 85–92, <https://doi.org/10.1016/j.jpowsour.2007.03.061>.
- [44] L. Han, *Aging and Degradation of Ion-Exchange Membranes*, Springer International Publishing, Cham, 2021, pp. 27–38, <https://doi.org/10.1007/978-3-030-41295-1>.
- [45] M.B. Andersen, M. van Soestbergen, A. Mani, H. Bruus, P.M. Biesheuvel, M. Z. Bazant, Current-induced membrane discharge, *Phys. Rev. Lett.* 109 (2012) 108301, <https://doi.org/10.1103/PhysRevLett.109.108301>.